

METALLIC COMPONENTS REPAIR STRATEGIES USING THE HYBRID MANUFACTURING PROCESS

Xinchang Zhang *, Wenyuan Cui *, Wei Li *, Frank Liou *

*Department of Mechanical & Aerospace Engineering
Missouri University of Science and Technology, Rolla, Missouri, 65409

Abstract

The hybrid manufacturing process which integrates additive manufacturing with subtractive machining is competitive and promising in component repair. To automate this process, detecting the missing volume and generating the deposition tracks is the key. In this study, strategies for repairing defects on flat and non-flat surfaces were investigated. A cost-effective reverse engineering tool was utilized to reconstruct STL models of damaged objects. Point data of the fracture surface on flat surfaces was obtained to generate the tool path for material building up. For defects on non-flat surfaces, the damaged model was best-fitted with the nominal model. Then both models were sliced and by using area comparison method, the defective domain was detected. Then a series of projection rays were utilized to slice the damaged cross-sections to extract the repair volume. Finally, repair experiments were performed to assess the repair quality through repair automation.

Keywords: Hybrid Manufacturing, Defect Repair, Laser Metal Deposition, Reverse Engineering

1. Introduction

Components of jet engines, airfoils, piping systems, heavy duty machines, molds and dies are usually working under harsh conditions. These conditions include intense heat, rapid heating and cooling cycles, dynamic contact, vibration, overload, severe impact, friction, erosion, and fatigue, etc. [1], [2]. Therefore, a large number of parts can be prematurely damaged and show several types of defects after a number of operation cycles. In general, the damaged parts exhibit defects in types of partial fracture, surface pits, scratches, cracking, peeling, distortion and spot corrosion, etc. [3]. Due to such flaws, damaged components such as impaired turbine blades and airfoils should be replaced since they can significantly reduce the performance of the aircraft, reduce engine fuel efficiency and even cause safety problems [4]. Dies and molds which are commonly utilized for mass production should preserve highly precise geometric dimensions. Worn dies and molds which beyond their acceptable tolerance are required to be substituted otherwise the manufactured products will carry defects inherently. However, replacing worn parts is not efficient because many high-performance parts are made of costly materials, e.g., Titanium alloys and Ni-based alloys, which also require special tools for machining, further increasing the manufacturing cost [5]. Replacing with new parts while discarding of worn ones is not only costly but also not an environmentally benign process. Besides, it is possibly difficult to find some parts in the market for historical machines. Therefore, it is significant to seek repair processes to restore damaged parts in order to maximize their service life.

Many worn parts can be successfully repaired to restore a satisfying or even better performance through several processes such as Tungsten Inert Gas Welding [6], Cold Spray [7]

and Laser Metal Deposition (LMD) [8], [9]. Among them, LMD process is widely interested due to many advantages, including (1) LMD process causes minimal dilution and small heat-affected area, which is preferred for repairing dimensional sensitive parts such as jet engine blades where shape dimensions are crucial [10]. (2) A good metallurgical bond can be formed between as-deposited material and base metals [11]. (3) LMD process can be integrated with CNC or robot to automate the repair process [12]. By using automation, the reliability, repeatability and quality of the repair process can be highly improved. (4) Many previously considered non-repairable components by conventional methods can be successfully repaired by LMD process [13]. (5) LMD process is compatible with many advanced materials [14].

LMD process belongs to a variety of solid free-form fabrication processes that can build fully dense parts by melting delivered metal particles using a laser source moving along a designed tool path (Fig. 1). Hybrid manufacturing is the integration of additive manufacturing such as LMD process with subtractive manufacturing such as CNC machining. LMD process can deposit adequate materials on the damaged region of a worn part. Extra materials can be machined using subtractive manufacturing to regain the designed dimensions and surface finish. The hybrid manufacturing process enhances the feasibility of repairing structurally complicated parts [15].

In component repair process, filler materials in shape of particles are delivered into the defective region and melted by a focused laser beam. Materials are added up in the damaged area along a defined route to regain the missing volume's geometry. Therefore, regenerating the missing volume's 3D model is the key to providing laser scanning tool path. Traditional LMD repair process relies on manual operation, i.e., the location, orientation, and geometry of the damaged portion must be defined manually and the laser scanning tool path is generated accordingly. Since components usually show diverse defects as the working environment is unique for each part, defining the missing geometry manually is inefficient, time-consuming and even impossible for complicated parts.

Automated defects reconstruction methods have been studied previously [16]–[18]. Wilson et al. provided a method to regain the repair volume by generating the fracture surface of the damaged blade to cut the nominal model [16]. Zheng et al. proposed an algorithm to extract the broken domain by calculating the distance of each point from the RE-generated damaged model to the surface of the nominal model [17]. Gao et al. used a surface extension method to regain the missing tip of a blade. However, the aforementioned studies were mainly focusing on repairing engine blades and has limitations for repairing other parts due to varied defects. What is more, too many calculations were performed on the point cloud which put the worn area modeling process inefficient. Using laser displacement sensor to directly scan damaged portion and generate repair volume was studied in [19]. However, using laser displacement sensor to measure coordinates of numerous points on the damaged portion slows down the repair process. What is more, the process was only focused on repairing defects located on a flat surface.

It should be noted that, although each component may have unique defects, the types of defects are usually limited, such as surface pits, dents, worn and partial fracture (like cracking). For repairing each type of defect, there may exist general defect reconstruction strategy to regain the missing volume with less time-consuming. In this study, parts with defects of surface dents and partial fracture were presented to explore the repair strategies. A cost-effective Reverse Engineering (RE) tool was utilized to generate models of the physically damaged parts. Based on the geometry and location of the damaged region, two defect reconstruction methods were

proposed to generate the repair volume. Then tool path of the missing volume was generated. LMD experiments were conducted to deposit proper materials on the damaged portion. After that, extra deposited materials were machined. Repaired parts were sectioned using an EDM to reveal the cross-section of deposits. Optical micrographs of the sectioned samples were obtained in order to assess the repair quality.

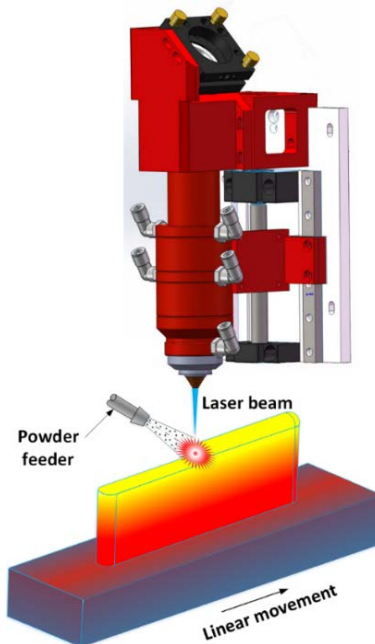


Fig. 1 Laser metal deposition process

2. Model reconstruction

Reconstructing the 3D model of the damaged part is the crucial step to obtain the model of the defective area. RE is usually used to generate the model of an existing object. Generally, RE-based scanning equipment can be classified into two categories: contact and non-contact. Coordinate measurement machines (CMMs) use probes to touch the physical object to measure the point cloud coordinates. Usually, contact-based scanners have the ability to scan transparent objects while low model acquisition speed is a major drawback. Non-contact scanners such as laser scanners and structured light scanners can generate the model in a very short time. However, the accuracy of the scanning process is highly affected by the properties of the object. Transparent and mirror-reflective objects should be well prepared before the scanning process.

In this study, models of the damaged parts were created using image stitching method processed in Autodesk Remake software. The process requires taking a number of images around the object using a camera (Fig. 2). In the process, the ready-to-scan object was located on a revolving stage for rotating the object in a constant interval such as 10 degrees and an SLR camera was fixed during the scanning process. Two orientations for the SLR camera were required. Side surfaces of objects can be captured by the camera in orientation A and the top surface of objects can be viewed by the camera in orientation B. The captured images (approximate 70 images for each part) were uploaded to the software to generate a 3D model. The output format of models in this study is STL (Stereolithography). A 30-mm length gage block was utilized to assess the accuracy of the process. It was found that the maximum error was 0.15 mm. The advantages of this

process include less equipment investment, ease of operation, fast model reconstruction speed and an acceptable accuracy. Fig 3 shows a physical part and the STL model reconstructed using the aforementioned method.

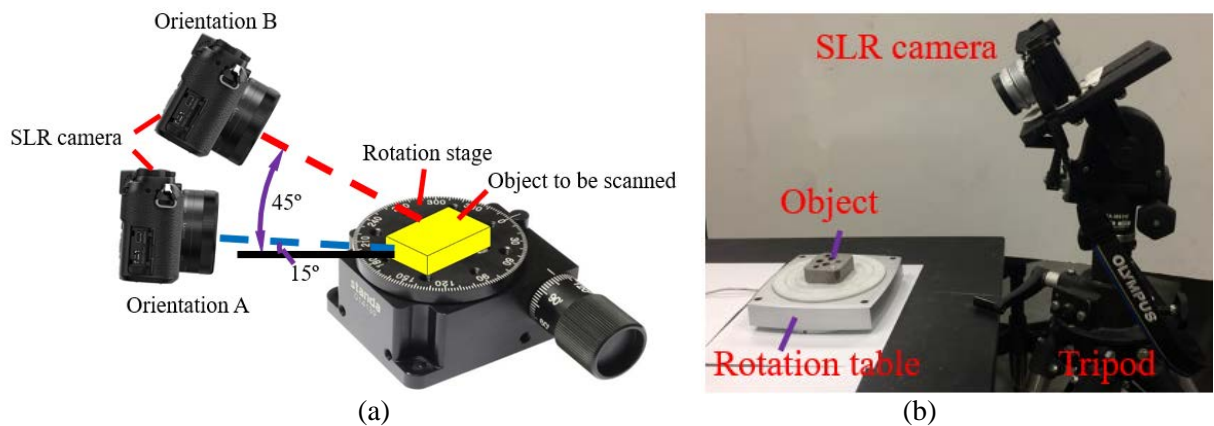


Fig. 2 Experimental setup for image capturing; (a) Schematic; (b) Equipment used

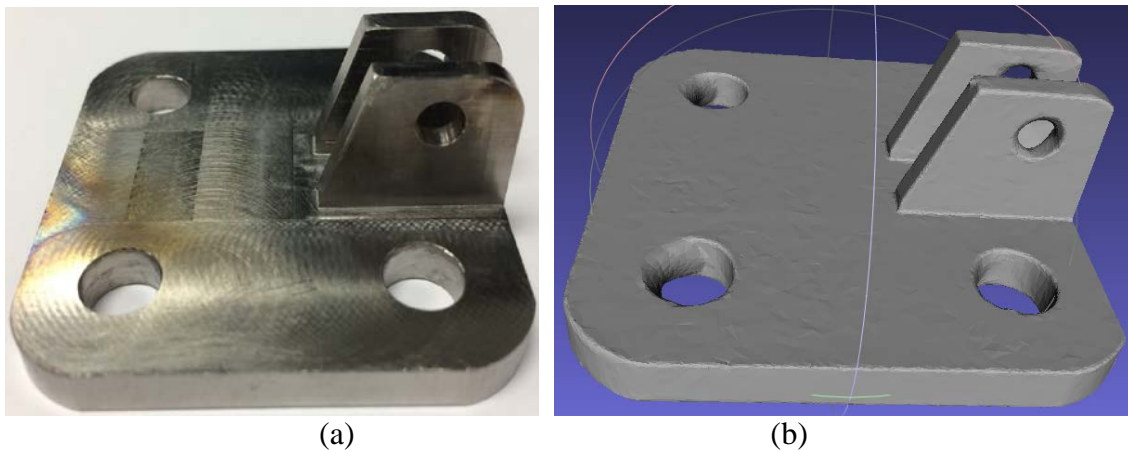


Fig. 3 A physical part (a) and reconstructed STL model (b)

3. General structure of component repair process

Four parts with defects of dents and partial fracture were presented to explore the repair strategies. Two parts (a plate and a die) have a flat surface and indentation-shaped defects were created on the flat surface. For another two parts (a cone and a jet engine blade), defects were located on a non-flat irregular surface. Based on the shape and location of defects, two strategies were proposed for obtaining the repair volume. The overall procedure is illustrated in Fig. 4. At first, damaged models of parts were reconstructed. For repairing the dents on a plate and a die, the point cloud of the fractured boundary surface was obtained through the reconstructed model. The point cloud was then processed to generate the tool path for material building up. In this case, the nominal model was not required. However, for repairing some parts such as the cone and the blade presented in this study, the repair volume cannot be defined directly without referring to the nominal model. In this case, the damaged model must be compared with the nominal model to extract the damaged region. Therefore, the damaged model was at first aligned with the nominal model. Then both models were sliced and an area comparison method was used to detect the defective region. Subsequently, casting rays were used to slice each damaged cross-section to

extract the missing volume. Then, tool path was generated according to the repair volume and repair experiments were conducted at last.

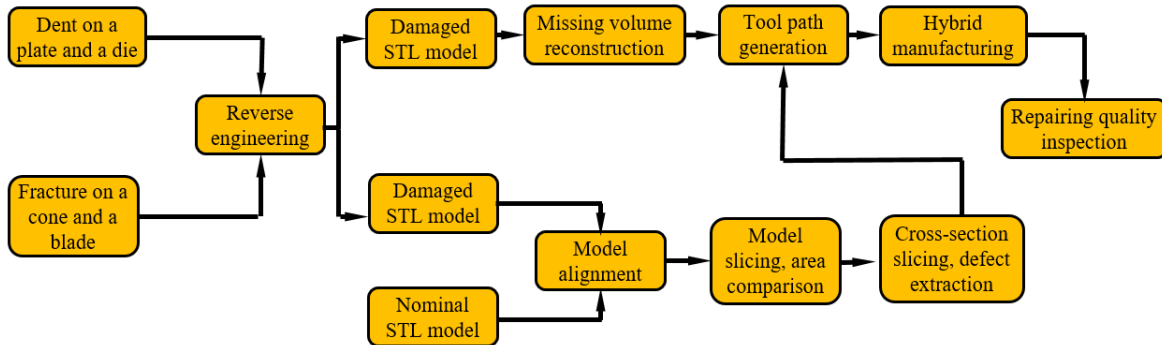


Fig. 4 General structure of automated defects repairing process

3.1. Case 1: Strategy for repairing defects on flat surfaces

Dents on the metal parts are usually caused by impact with other objects. As shown in Fig. 5 (a), a 15-mm diameter ball end mill defect was created on the top flat surface of a plate to a depth of 3 mm to simulate the impact defect. Considering the geometry and location of the defect, it can be seen that the missing volume is surrounded by the boundary fracture surface and a missing flat top surface. Therefore, the repair volume can be defined by measuring the point coordinates of the fracture surface. Previously, the point cloud coordinates can be generated by probing with a coordinate measurement machine (CMM) or a laser displacement sensor, which requires significantly longer time in the data acquisition process. In this research, the process shown in Fig. 2 was adopted to reconstruct the model of the damaged components.

The reconstructed STL model of the damaged plate was shown in Fig. 5 (b). It was found that both holes at the end of the diagonal are different from the physical object. However, since both holes were not located in the damaged region, they have no effects on the defect reconstruction and repair process.

The point cloud of the boundary fracture surface was extracted as shown in Fig. 6 (a). After that, the point cloud was sliced into five layers and the convex hull of each layer was calculated. Subsequently, raster deposition tool path was generated as shown in Fig. 6 (b), which consists of effective deposition path and turning path with laser powered off.



Fig. 5 (a) A damaged plate with a ball indentation; (b) Reconstructed model of the damaged plate

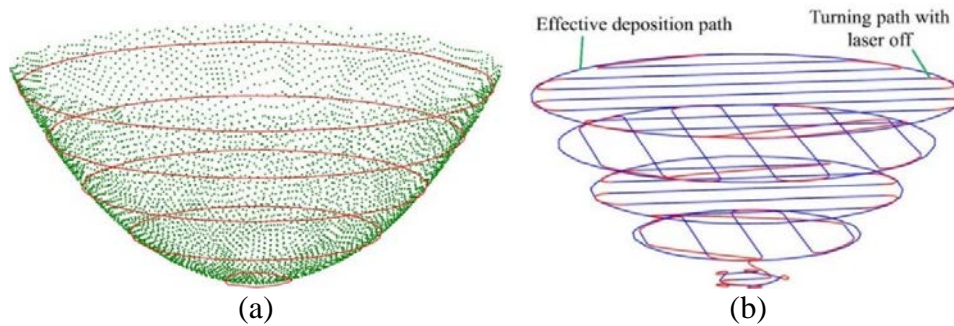


Fig. 6 Deposition path generation. (a) The point cloud of the boundary surface of the defective area and layered convex hull; (b) Deposition tool path

An H13 tool steel die with a ball indentation was also used to test the repair strategy (Fig. 7). Similarly, the missing volume of the die can be regained by capturing the point cloud of the boundary fracture surface. For this purpose, the 3D reconstructed model of the die was generated as shown in Fig. 7 (b). The point cloud of the fracture surface was extracted and then processed to generate the deposition tool path as shown in Fig. 7 (c).

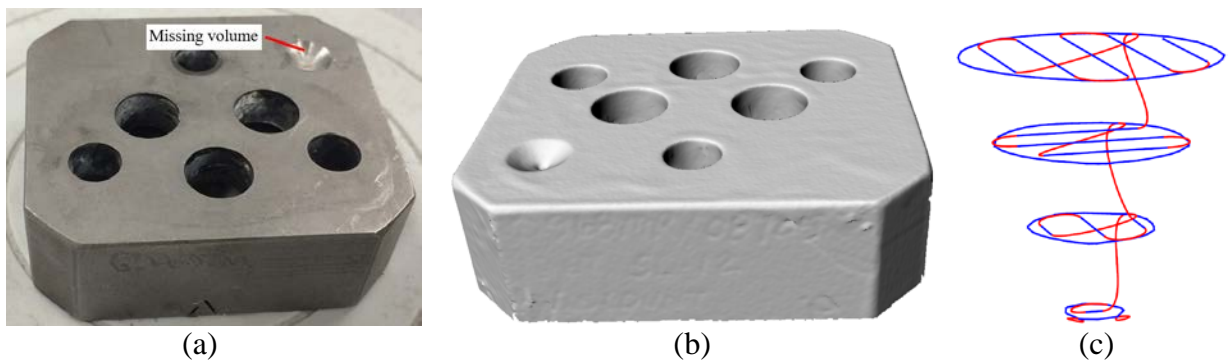


Fig. 7 (a) An H13 tool steel die with a ball indentation; (b) Reconstructed model of the damaged die; (c) Deposition tool path

3.3. Case 2: Strategy for repairing defects on non-flat surfaces

In case 1, it can be seen that the top surface of the damaged part is a flat surface, which makes the defect detection and reconstruction process straightforward. The nominal model without defects is not needed to define the repair volume. However, in most cases, the worn part must be compared with its nominal part to detect and extract the damaged region. To investigate the strategy for repairing those parts, an original intact cone and partially fractured cone as shown in Fig. 8 were used to present the proposed strategy. The defect was located on the side surface of the cone. The inner surface of the missing volume can be defined by measuring the point cloud fracture surface. However, the outer surface of the defect cannot be determined directly from the damaged model. An algorithm is required to compare the damaged model with the nominal model to extract the defective area.

The proposed defect modeling algorithm includes the following steps: (1) Model acquisition; (2) Model best-fit; (3) Defect detection; (4) Defect extraction. The detailed steps were presented below.

Step 1: Model Acquisition. For this cone example, in order to demonstrate the feasibility of the proposed strategy, both the nominal and damaged models were obtained through CAD-generated STL models and were shown in Fig. 8. In real applications, the damaged model can be obtained through RE. The nominal model can be acquired from RE or CAD database.

Step 2: Model best-fit. For RE generated model, the reconstructed damaged model is usually in arbitrary position and orientation with the nominal model. Therefore, the damaged model must be aligned with the nominal model for the defect detection and extraction purpose.

Step 3: Defect detection. A series and equidistant references which are parallel to the bottom surface of the cone were utilized to slice the nominal and damaged models. The sliced models were shown in Fig. 9. Then the area of each cross-section of the nominal model and damaged model were calculated and compared. If the area difference of one layer was beyond a pre-set tolerance, that layer on the damaged model was in the damaged region. After this step, the damaged layers of the worn model can be detected as shown in Fig. 9 (b).

Step 4: Defect extraction. As shown in Fig. 10, a series of projection rays ($l_1, l_2, l_3 \dots$) were used to slice the damaged cross-section of the damaged model and corresponding layer of the nominal model. The intersections of each ray with the damaged cross-section were obtained as $a_1, b_1, a_2, b_2, a_3, b_3 \dots$. The intersections of each ray with the nominal cross-section were $m_1, n_1, m_2, n_2, m_3, n_3 \dots$. The value of each intersection from damaged cross-section can be compared with the corresponding intersection from the nominal cross-section, for instance, a_1 compared with m_1 . If the difference between two intersections was beyond a tolerance (for example, n_3, b_3), these two intersections were recorded. It can be seen that these intersections enveloped the missing volume. The process continues through each cross-section as shown in Fig. 11. Finally, the missing volume can be obtained as shown in Fig. 12.

This process was also adopted to detect and extract a fractured area of a jet engine compressor blade as shown in Fig. 13. A defect was cut on the blade edge to simulate the impact of blades with foreign objects (birds, rocks...). Through defect detection process, the damaged layers of the blade were obtained as shown in Fig. 14 (a). The missing volume was then extracted as shown in Fig. 14 (b). Deposition tool path was generated based on the extracted missing volume and was shown in Fig. 14 (c).

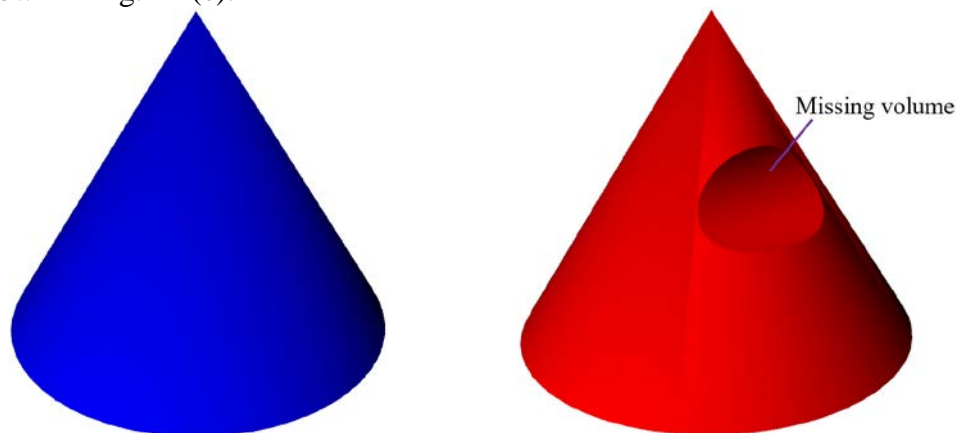


Fig. 8 (a) Nominal model of the original cone; (b) Damaged model of the damaged cone

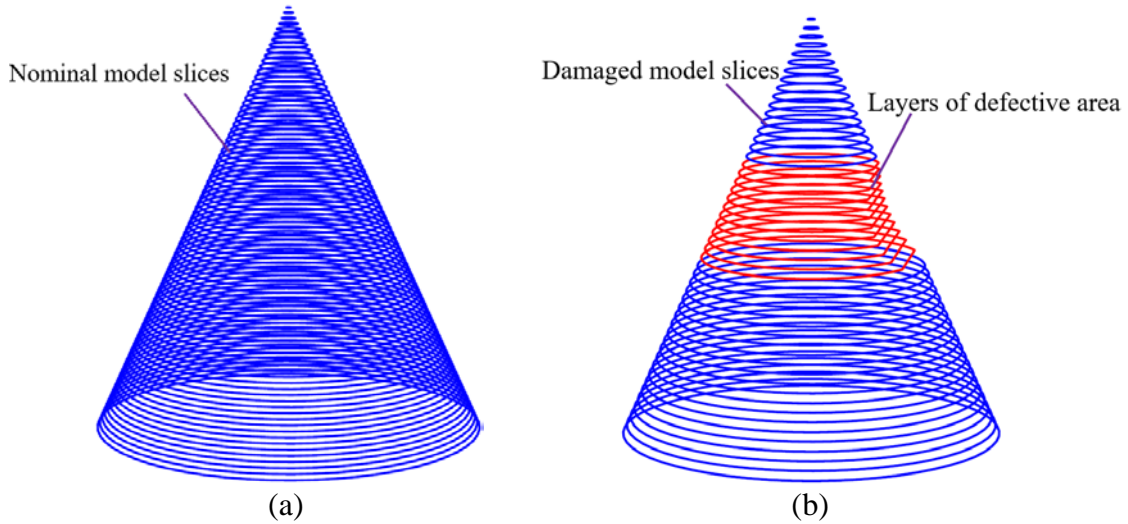


Fig. 9 (a) Cross-sections of the nominal model; (b) Cross-sections of the damaged model;

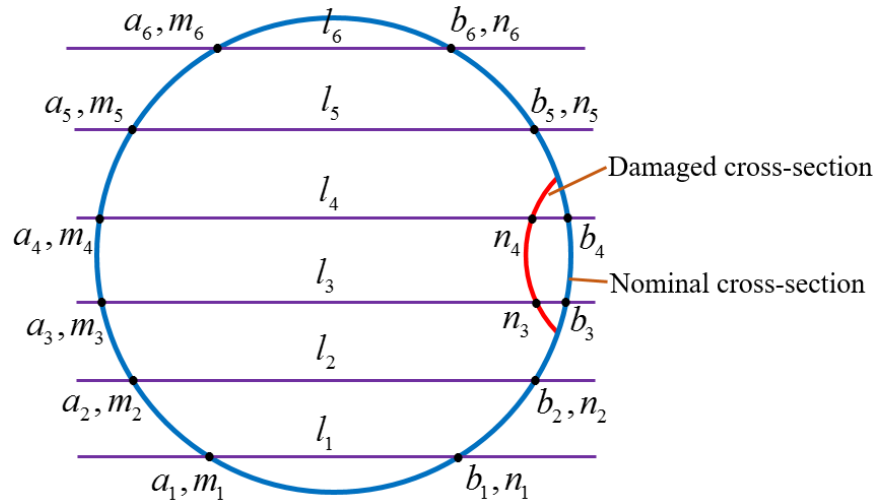


Fig. 10 Cross-sections of the nominal and damaged models and intersections with projection rays

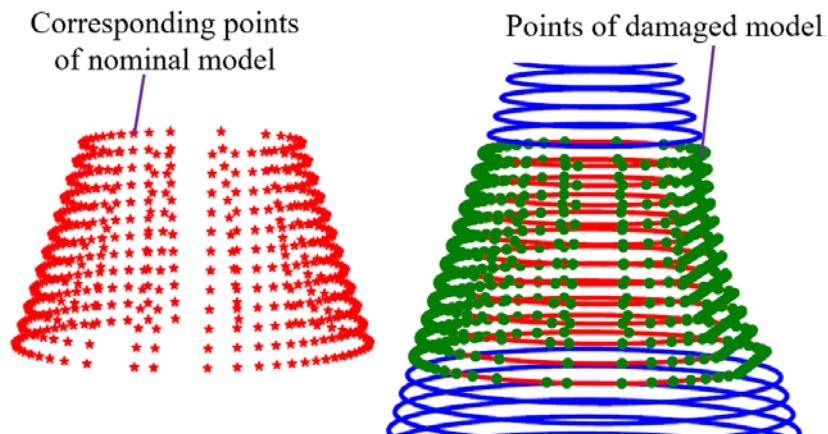


Fig. 11 Intersections of projection rays with cross-sections of the nominal and damaged models

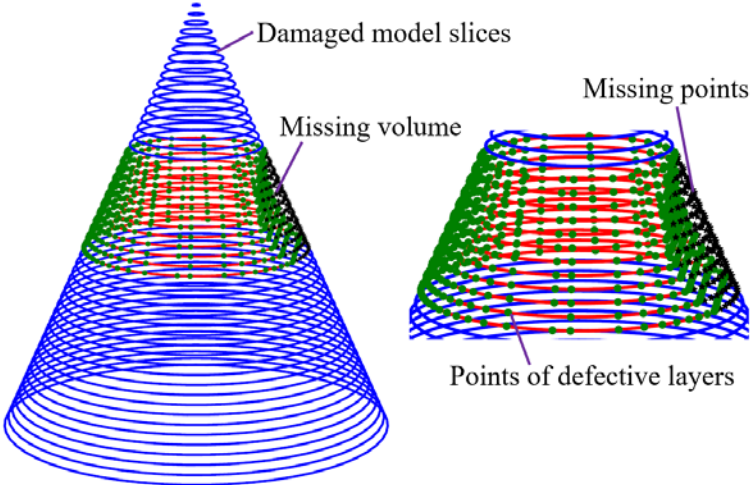


Fig. 12 Reconstructed missing volume boundary points

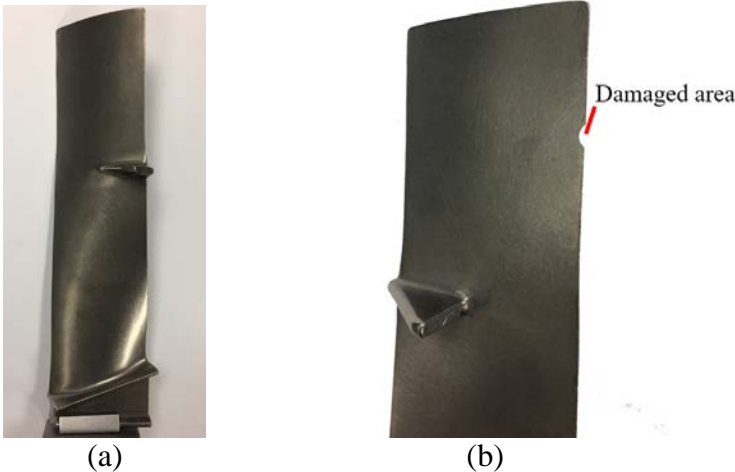
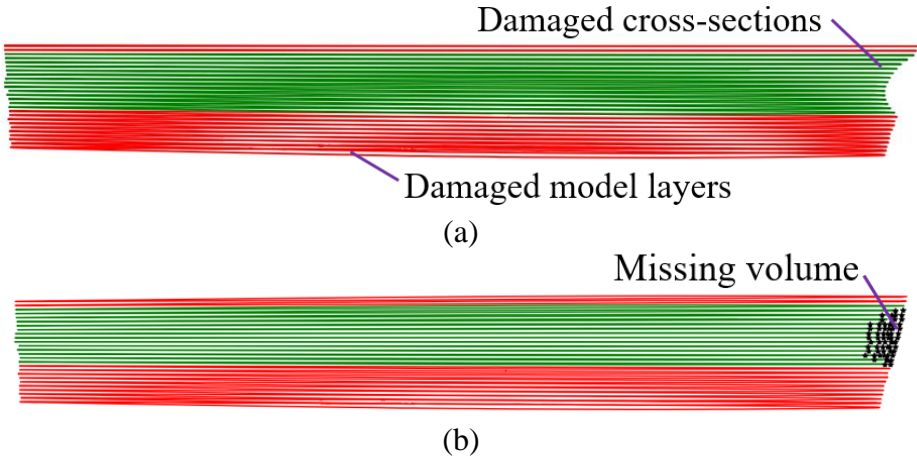
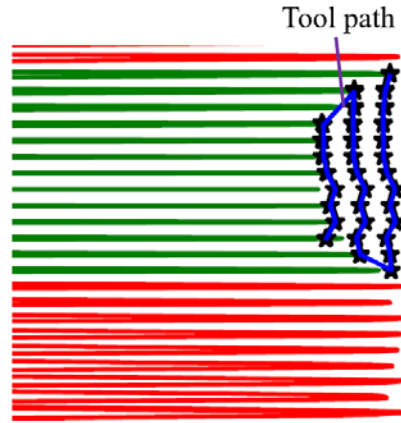


Fig. 13 (a) Nominal blade; (b) Damaged blade





(c)

Fig. 14 (a) Blade defect detection; (b) Blade defect extraction; (c) Tool path generation

4 Repair experiments

4.1 Experimental setup and materials preparation

In this study, the repair process was performed using the hybrid manufacturing process. The laser metal deposition system (Fig. 15) consists of laser source, powder feeding system, motion control system and gas feeding system. A peak of 1000 W fiber laser from IPG Photonics was used as the heat generator. The laser beam diameter was 1.8 mm. A powder feeding system from Bay State Surface Technologies (Model 1200) was utilized for delivering powder to the melting pool created by the laser beam. The powder feeding nozzle was vertical while the laser beam was tilted. The initial distance between the nozzle and the substrate was 10 mm. Relative movement between damaged parts and the laser beam was realized by a 3-axis motion table. Argon gas was used as the powder delivery gas and shielding gas to protect the deposited material from oxidation.

The defective area of damaged parts was cleaned using acetone before the repair process. The filler materials for repairing the steel plate, AISI H13 tool steel die and Ti-6Al-4V blade were Inconel 625, Cobalt-based alloy Wallex 40 and Ti-6Al-4V, respectively. Micrographs of target particles were taken using a Field Emission Scanning Electron Microscopy (Hitachi S4700) and were shown in Fig. 16. It can be found that most powders were spherical although some irregularly shaped powders were detected. The chemical composition of filler materials was listed in Table 1. The processing parameters for LMD process were listed in Table 2.

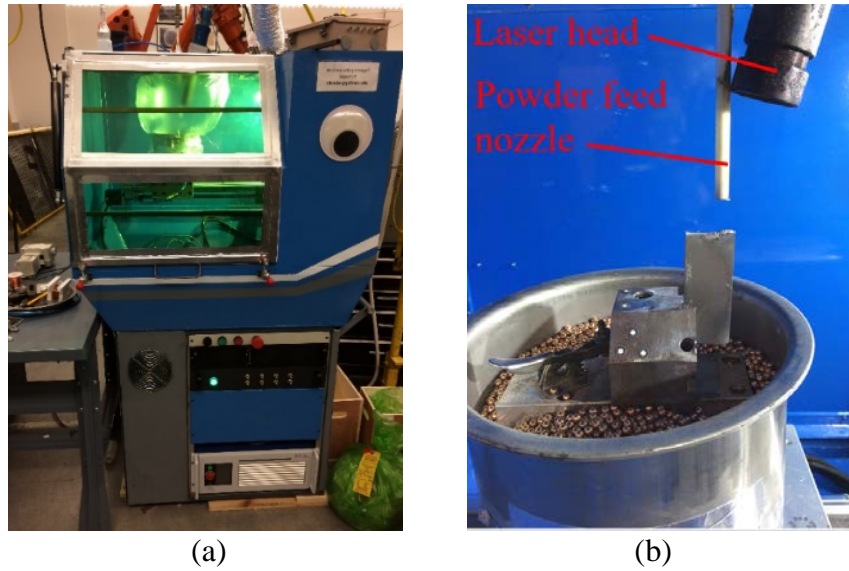


Fig. 15 (a) The LMD system; (b) Experimental set-up

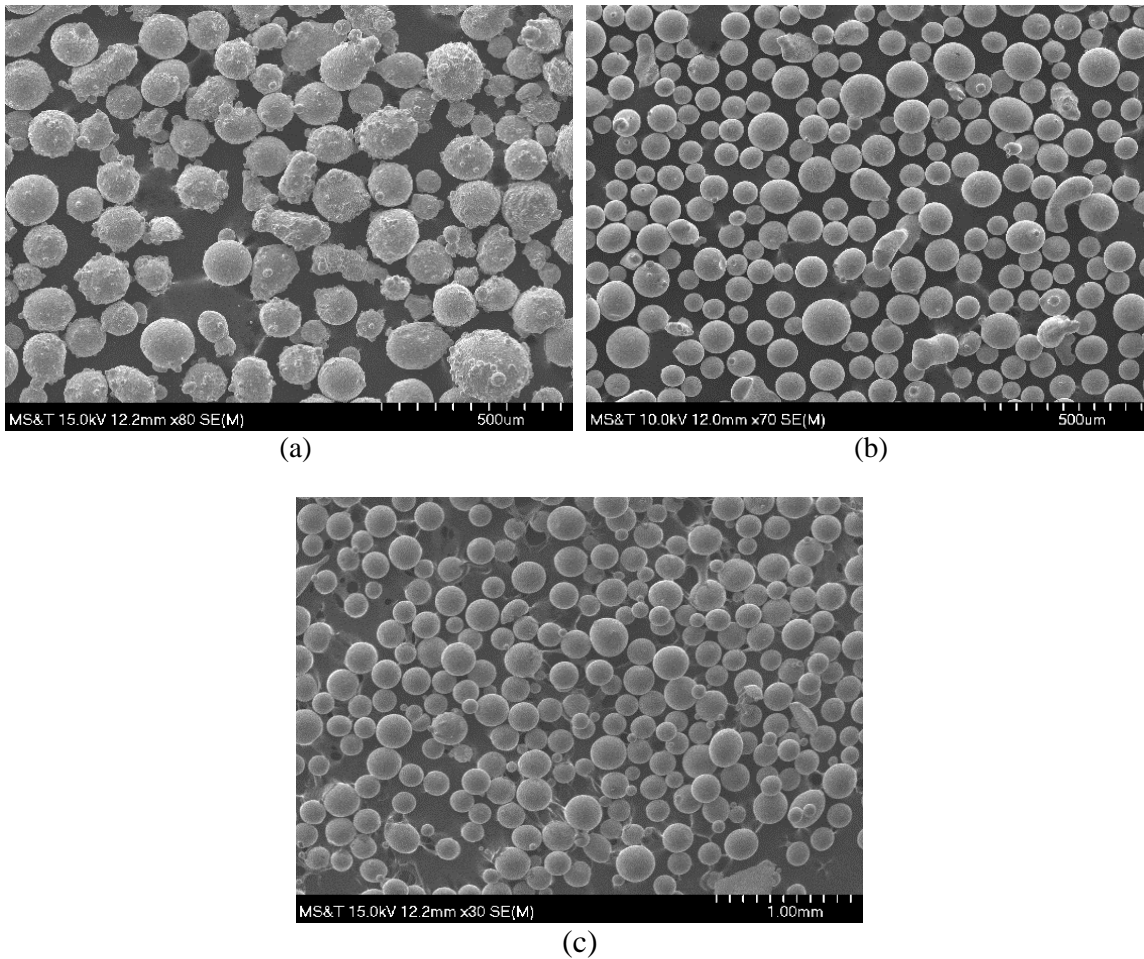


Fig. 16 SEM images of (a) Inconel 625, (b) Wallex 40 and (c) Ti-6Al-4V particles

Table 1 Chemical composition of the target materials (Wt %)

Materials	Ni	Co	Ti	C	Mn	Si	Cr	Fe	Mo	V	W	B	Al	N
-----------	----	----	----	---	----	----	----	----	----	---	---	---	----	---

Inconel 625	Bal.	3.5	-	1.0	0.3	0.25	21.5	4	9.0	0.25	-	-	-	-
Wallex 40	23.5	Bal.	-	0.6	-	1.9	16.2	1.3	-	-	7.6	2.0	-	-
Ti-6Al-4V	-	-	Bal.	≤ 0.08	-	-	-	≤ 0.4	-	3.5-4.5	-	-	5.5-6.75	≤ 0.05

Table 2 LMD processing parameters

Part	Laser power (W)	Scan speed (mm/min)	Powder feed rate (g/min)	Track overlap (%)
Plate	400	200	3.2	0.5
Die	600	200	2.8	0.5
Blade	300	200	2.5	0.5

4.2 Repair results and discussion

Fig. 17 (a) shows the plate after laser metal deposition and before machining. Extra material was removed by flattening the top surface and the plate was shown in Fig. 17 (b). The amount of material being removed was defined from the nominal model. The repaired plate was sectioned using EDM to reveal the cross-section in order to assess the repair quality. The micrograph of the cross-section of the plate taking using HIROX KH-8700 optical microscope was shown in Fig. 17 (c). It can be seen that the filler material was deposited successfully on the defective area. Only a few micropores were discovered in the deposited material. The interface was very clear and no defects were found.

Fig. 18 (a) and (b) show the repaired die before and after finish machining. The optical micrograph of the cross-section of the die was shown in Fig. 18 (c). The Wallex 40 deposits show a dense microstructure. The interface was intact and a good metallurgical bond was formed. Fig. 19 (a) and (b) show the blade after deposition and after machining, respectively. The repair result and microstructure analysis demonstrated that the proposed defect repair strategies were suitable and efficient for automated component repair.

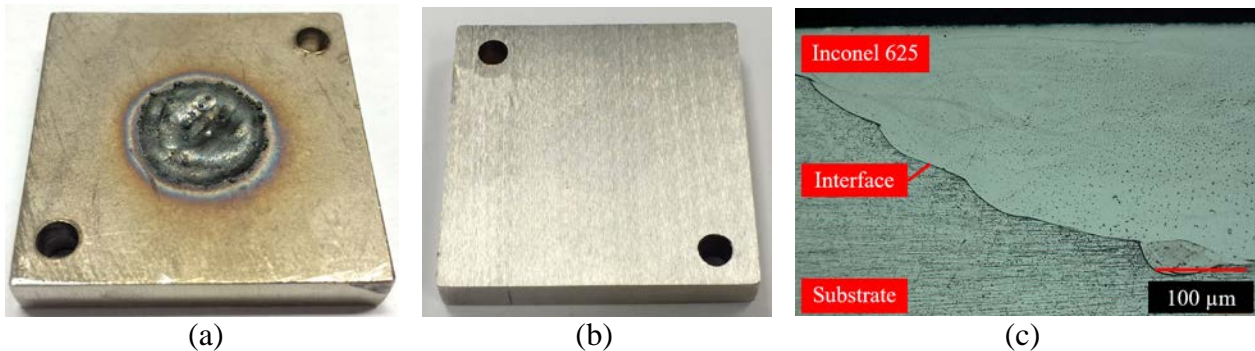


Fig. 17 Plate repair result. (a) Plate after LMD process; (b) Plate after machining; (c) Optical micrograph of cross-section of the plate

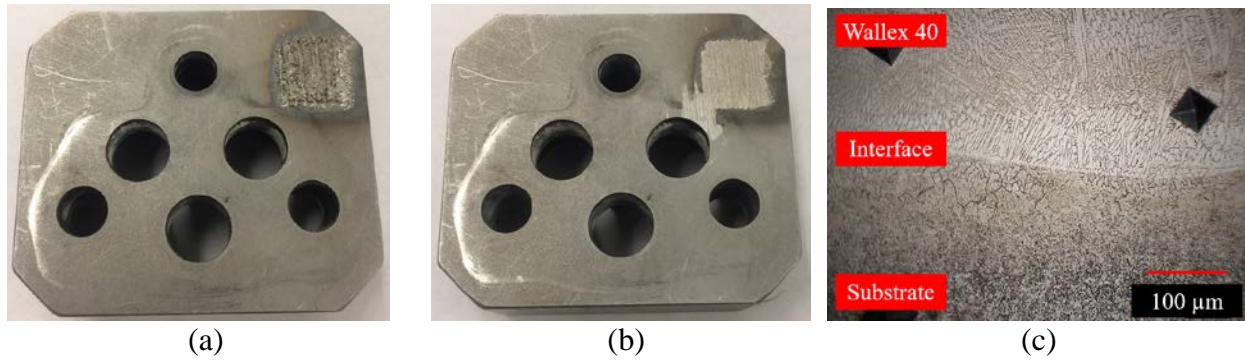


Fig. 18 Die repair result. (a) Die after LMD process; (b) Die after machining; (c) Optical micrograph of cross-section of the die

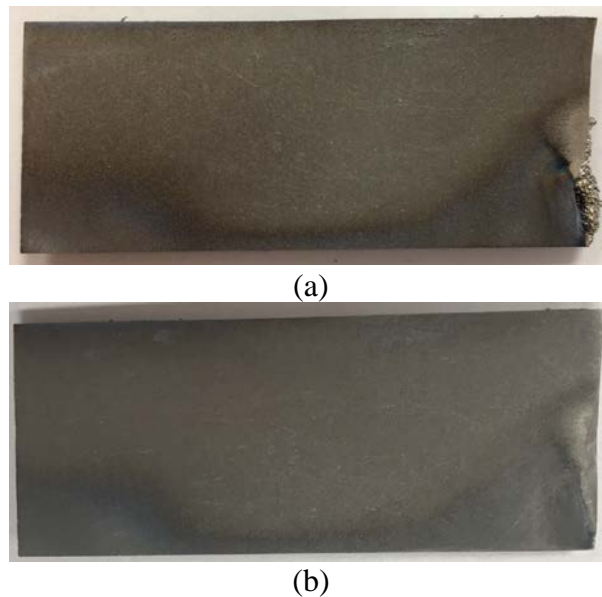


Fig. 19 Blade repair result. (a) Blade after LMD process; (b) Blade after machining.

4. Conclusion

Strategies for automated extracting the repair volume on flat and non-flat surfaces were investigated in this study. Based on the geometry and location of the damaged region, two repair strategies were presented to balance the repair feasibility and efficiency. Each strategy takes the RE reconstructed model as the input. For repairing defects on a flat surface, the repair volume was enclosed by the fractured boundary surface. The coordinates of point cloud on the boundary surface were obtained through the reconstructed STL models. The nominal model is not required in this case. For obtaining the damaged domain on a non-flat surface, a strategy was introduced including the following steps: (1) Model acquisition, (2) Model best-fit, (3) Defect detection and (4) defect extraction. At first, both the damaged and nominal models were obtained. Then the damaged model was best-fitted with the nominal model. After that, both models were sliced by a series and equal distant references. A number of cross-sections of both models were obtained. The area of the cross-section of the damaged and nominal models was calculated and compared. If the area difference was beyond a tolerance, the cross-section on the damaged model was located in the defective region. After this step, the damaged layers of the damaged model can be defined. Finally, a series of

projection rays were used to slice each damaged cross-section and corresponding nominal cross-section to extract the repair volume. Deposition tool path was generated by slicing the defective area into layers. Three physical damaged objects were repaired using the hybrid manufacturing process. Cross-sections of the repaired parts were analyzed using an optical microscopy. The repair experiments and analysis validated the feasibility of the repairing strategies presented in this paper.

Acknowledgement

This project was supported by National Science Foundation Grants CMMI-1547042 and CMMI 1625736, and the Intelligent Systems Center, Center for Aerospace Manufacturing Technologies, and Material Research Center at Missouri S&T. Their financial support is greatly appreciated.

Reference

- [1] M. A. Zavareh, A. A. D. M. Sarhan, B. B. A. Razak, and W. J. Basirun, "Plasma thermal spray of ceramic oxide coating on carbon steel with enhanced wear and corrosion resistance for oil and gas applications," *Ceram. Int.*, vol. 40, no. 9 PART A, pp. 14267–14277, 2014.
- [2] J. H. LEE, J. H. JANG, B. D. JOO, Y. M. SON, and Y. H. MOON, "Laser surface hardening of AISI H13 tool steel," *Trans. Nonferrous Met. Soc. China (English Ed.)*, vol. 19, no. 4, pp. 917–920, 2009.
- [3] S. Jhavar, C. P. Paul, and N. K. Jain, "Causes of failure and repairing options for dies and molds : A review," *Eng. Fail. Anal.*, vol. 34, pp. 519–535, 2013.
- [4] T. Blades, "Detc2011-48652 Virtual Repair : Geometric Reconstruction for Remanufacturing Gas," *Proceeding ASME 2011 Int. Des. Eng. Tech. Conf.*, pp. 1–10, 2011.
- [5] A. Pramanik, "Problems and solutions in machining of titanium alloys," *Int. J. Adv. Manuf. Technol.*, vol. 70, no. 5–8, pp. 919–928, 2014.
- [6] K. Nakata *et al.*, "Re-weldability of neutron-irradiated stainless steels studied by multi-pass TIG welding," *J. Nucl. Mater.*, vol. 307–311, no. 2 SUPPL., pp. 1578–1583, 2002.
- [7] V. Champagne and D. Helfritsch, "Critical Assessment 11: Structural repairs by cold spray," *Mater. Sci. Technol.*, vol. 31, no. 6, pp. 627–634, 2015.
- [8] H. Qi, M. Azer, and P. Singh, "Adaptive toolpath deposition method for laser net shape manufacturing and repair of turbine compressor airfoils," *Int. J. Adv. Manuf. Technol.*, vol. 48, no. 1–4, pp. 121–131, 2010.
- [9] B. Graf, A. Gumenyuk, and M. Rethmeier, "Laser metal deposition as repair technology for stainless steel and titanium alloys," *Phys. Procedia*, vol. 39, pp. 376–381, 2012.
- [10] O. Yilmaz, N. Gindy, and J. Gao, "A repair and overhaul methodology for aeroengine components," *Robot. Comput. Integr. Manuf.*, vol. 26, no. 2, pp. 190–201, 2010.
- [11] Q. Wu, W. Li, N. Zhong, W. Gang, and W. Haishan, "Microstructure and wear behavior of laser cladding VC–Cr7C3 ceramic coating on steel substrate," *Mater. Des.*, vol. 49, pp. 10–18, 2013.
- [12] J. Ruan, K. Eiamsa-ard, and F. W. Liou, "Automatic Process Planning and Toolpath Generation of a Multiaxis Hybrid Manufacturing System," *J. Manuf. Process.*, vol. 7, no. 1, pp. 57–68, 2005.
- [13] A. Uriondo, M. Esperon-Miguez, and S. Perinpanayagam, "The present and future of additive manufacturing in the aerospace sector: A review of important aspects," *Proc. Inst. Mech. Eng. Part G J. Aerosp. Eng.*, vol. 229, no. 11, pp. 2132–2147, 2015.
- [14] D. D. Gu, W. Meiners, K. Wissenbach, and R. Poprawe, "Laser additive manufacturing of metallic components: materials, processes and mechanisms," *Int. Mater. Rev.*, vol. 57, no.

- 3, pp. 133–164, 2012.
- [15] F. Liou, K. Slattery, M. Kinsella, J. Newkirk, H. Chou, and R. Landers, “Applications of a hybrid manufacturing process for fabrication of metallic structures,” *Rapid Prototyp. J.*, vol. 13, no. 4, pp. 236–244, 2007.
 - [16] J. M. Wilson, C. Piya, Y. C. Shin, F. Zhao, and K. Ramani, “Remanufacturing of turbine blades by laser direct deposition with its energy and environmental impact analysis,” *J. Clean. Prod.*, vol. 80, pp. 170–178, 2014.
 - [17] J. Zheng, Z. Li, and X. Chen, “Worn area modeling for automating the repair of turbine blades,” *Int. J. Adv. Manuf. Technol.*, vol. 29, no. 9–10, pp. 1062–1067, 2006.
 - [18] J. Gao, X. Chen, O. Yilmaz, and N. Gindy, “An integrated adaptive repair solution for complex aerospace components through geometry reconstruction,” *Int. J. Adv. Manuf. Technol.*, vol. 36, no. 11–12, pp. 1170–1179, 2008.
 - [19] R. Liu, Z. Wang, T. Sparks, and F. Liou, “Stereo Vision Based Hybrid Manufacturing of Ti-6Al-4V in Component Repair Process,” *2014 Annu. Int. Solid Free. Fabr. Symp.*, pp. 1425–1431, 2014.